Estuaries and Coasts (2011) 34:785–799
DOI 10.1007/s12237-011-9401-y

Characteristics of a Shallow River Plume: Observations from the Saco River Coastal Observing System

Charles E. Tilburg · Shaun M. Gill · Stephan I. Zeeman · Amy E. Carlson · Timothy W. Arienti · Jessica A. Eickhorst · Philip O. Yund

Received: 16 March 2010 / Revised: 3 December 2010 / Accepted: 2 April 2011 / Published online: 3 May 2011

Abstract Interest in the coastal dynamics of river plumes has mainly focused on large rivers, but plumes from the more numerous smaller rivers have important local consequences and may, in aggregate, be significant contributors to coastal circulation. We studied the dynamics of the plume from the Saco River in Saco Bay, Gulf of Maine, over a 3-year period. The transport and salinity in the region are governed by river discharge, tides, winds, and interaction with the Western Maine Coastal Current. The dynamics of the flow field vary with location within the plume and discharge. The far-field dynamics of the Saco River plume are dominated by inertial processes (hence qualifying it as a small-scale river plume), during times of low discharge, with low salinity water present both up and downstream of the river mouth, but are dominated by rotational processes during times of high discharge (thus qualifying it as a large-scale river plume), with buoyant water primarily advected downshelf. Near-field dynamics are governed by weak, subcritical flow during low discharge but strongly inertial, supercritical flow during high discharge. Offshore movement of the plume is not governed by Ekman dynamics but is instead a result of discharge, wind-induced vertical mixing, and the geography of the coastline and adjacent islands.

Keywords River plumes · Winds · Tides · Discharge · Observations · Estuaries · Shelf dynamics

C. E. Tilburg (✉) · S. M. Gill · S. I. Zeeman · A. E. Carlson · T. W. Arienti · J. A. Eickhorst · P. O. Yund
Department of Marine Sciences and Marine Science Center, University of New England,
11 Hills Beach Road,
Biddeford, ME 04093, USA
e-mail: ctilburg@une.edu

Introduction

The dynamics of the coastal ocean are inextricably linked to the terrestrial environment by rivers. River discharges produce buoyant plumes of freshwater that affect coastal circulation patterns and may carry nutrients, sediment, and contaminants that affect coastal food webs (Rabalais et al. 2000). Buoyant river plumes often extend over expansive areas (Lentz and Limeburner 1995) and affect transport and mixing for large distances downshelf of the mouth (Munchow and Garvine 1993). Biological processes in the coastal ocean are closely coupled to the dynamics of freshwater plumes. So, an understanding of the effects of river plumes on the coastal environment requires knowledge of both physical circulation and mixing processes.

The dynamics of river plumes have important implications for the transport of larvae, contaminants, nutrients, and pathogens (e.g., Venkatesan et al. 1998; Lipp et al. 2001; Schiff et al. 2003; Gersberg et al. 2004; Warrick et al. 2007; Nagvenkar and Ramalah 2009; Wargo et al. 2009). Coastal regions can be subject to episodic contamination during storm events from fecal bacteria emanating from rivers (Schiff et al. 2003). Understanding the transport of fecal bacteria within the plume, especially under conditions in which a shallow plume is advected onto shore, is thus critical for predicting human impacts along the shore. Rivers can influence the delivery of nutrients, the timing of delivery and their relative ratios to coastal waters and thus affect the productivity and species composition of coastal phytoplankton (e.g. Otero and Siegel 2004; Warrick et al. 2005). Similarly, toxic algal blooms can occur where nutrient-rich river plumes contact nearshore cyst beds (Anderson et al. 2005). Because rainfall and snow melt are strongly seasonal and exhibit interannual variation, river plumes and the biological processes that they influence

vary on time scales of days, months, years, and decades (e.g., Yanagi and Hino 2005; Thomas and Weatherbee 2006). Consequently, the understanding of the fate of freshwater discharge to the coastal ocean and the causes and consequences of the freshwater plumes has become a major goal of coastal oceanography (Henrichs et al. 2000).

While much work has focused on larger rivers (e.g., Munchow and Garvine 1993; Rabalais et al. 2000), the dynamics and characteristics of smaller rivers are still not well understood (Gaston et al. 2006). However, the dynamics of smaller river plumes are vital to processes on the local scales that are relevant to many management practices and the cumulative effect of the inflows from the more numerous smaller rivers may be as important as that of the less numerous larger rivers. Consequently, recent studies have begun to examine the fate of small rivers as they enter the coastal region (e.g. Warrick et al. 2007).

This study examines the dynamics of the Saco River plume, located in Saco Bay in the northwestern Atlantic, a region governed by wind-driven transport, tidal currents, and large-scale buoyancy forcing from the Gulf of Maine coastal current system (Pettigrew et al. 1998, 2005). Here, we determine the governing characteristics of the flow field and the physical mechanisms responsible for (1) the across-shelf extent of the Saco River plume, (2) transport and salinity within the plume, and (3) vertical mixing of the plume using data from the Saco River Coastal Observing System (SaRCOS) sensors and hydrographic transects of the Saco River plume and the adjacent coastal region.

Background

A number of modeling and theoretical studies have classified the dynamics responsible for the transport and mixing of buoyant plumes based on readily measured criteria (e.g. Garvine 1995; Yankovsky and Chapman 1997; Avicola and Huq 2001). Garvine (1995) classified buoyant plumes as "small-scale" or "large-scale" based on the relative contributions of inertial and rotational processes within the plume. Large-scale plumes tend to be more affected by the Earth's rotation than inertial dynamics. Large-scale plumes leave their source and turn downshelf (i.e. in the direction of Kelvin wave propagation), creating a geostrophically balanced coastal current (e.g. Chapman and Lentz 1994) that transports buoyant water downshelf of the mouth. In the absence of winds, little buoyant water is typically found upshelf of the mouth (Munchow and Chant 2000). Small-scale plumes are governed by inertial dynamics and tend to form freshwater bulges that radiate in all directions from the source (Garvine 1995), thus regularly producing low salinity upshelf of the source. Garvine (1995) used the bulk Kelvin number, K, a measure of the relative importance of rotational and inertial processes to classify the scale of the plumes. The bulk Kelvin number is expressed as:

$$K = \frac{R_p}{R_D} \tag{1}$$

where R_p is the observed across-shelf extent of the buoyant plume or coastal current and R_D is the radius of deformation:

$$R_D = \frac{\sqrt{g' h_p}}{f} \tag{2}$$

where h_p is the thickness of the plume, f is the Coriolis parameter, and $g' = g(\rho_{amb} - \rho_o)/\rho_o$ where g is gravitational acceleration, ρ_{amb} is the ambient ocean density, and ρ_o is the density of the incoming freshwater. Large Kelvin numbers ($K>>1$) are indicative of "large-scale" plumes, and small Kelvin numbers ($K<<1$) indicate "small-scale" plumes. While the Kelvin number is largely a geometric parameter that examines length scales of the plume, the Rossby number, R, is a dynamic parameter commonly used to compare inertial and rotational processes of a flow field. The Rossby number is expressed as:

$$R = \frac{u_c}{f R_D} \tag{3}$$

where u_c is a characteristic velocity of the flow. Large Rossby numbers ($R>>1$) indicate flow that is dominated by inertial processes, while small Rossby numbers ($R<<1$) indicate flow dominated by rotational processes.

Since plumes can be affected by winds and other frictional processes, the Ekman number, E_k, can be used to estimate the relative strengths of frictional and rotational processes and can be expressed as:

$$E_k = \frac{K_z}{f h_p^2} \tag{4}$$

where K_z is the vertical eddy viscosity. Large values of the Ekman number ($E_k>1$) indicate friction-dominated flow, while small values ($E_k<1$) indicate rotational flow (Cushman-Roisin 1994).

Chao (1988) used the Froude number to characterize the tendency of flow fields to be governed by baroclinicity or inertial processes. The Froude number, Fr, is expressed as

$$Fr = \frac{u_c}{\sqrt{g' h_p}} \tag{5}$$

Larger values of the Froude number ($Fr>>1$) correspond to supercritical flow in which inertial processes predominate and stratification processes are not important. Smaller values ($Fr \leq 1$) correspond to subcritical flow in which stratification is important (Cushman-Roisin 1994).

Since the dynamics that govern the flow vary depending on location within the plume (e.g., Chao and Boicourt 1986), these parameters can be calculated within the bulge of the plume, the coastal current emanating from the bulge, or the mouth itself. R and Fr can be calculated throughout the plume to examine how dynamics change within the plume. However, the mouth Kelvin number, K_m, requires a different length scale (here we use the mouth width, W, as the characteristic length scale). The mouth Kelvin number is defined here as (e.g. Huq 2009):

$$K_m = \frac{W}{R_D} \tag{6}$$

Tides (e.g. Simpson and Souza 1995; Sanders and Garvine 2001) can also affect the plume shape, thickness and location. A useful classification of estuaries by circulation and tidal mixing parameters is the effective ratio of the cross-sectionally averaged freshwater velocity to the average tidal current (Hansen and Rattray 1966). This tidal index, P, is expressed as:

$$P = \frac{(Q_R/h_0 W)}{u_t} \tag{7}$$

where Q_R is the river discharge, h_o is the average river mouth depth, W is the river mouth width, and u_t is the mean tidal speed. Large values of the tidal index ($P>1$) indicate a buoyancy governed flow, while small values of the tidal index ($P<1$) indicate tidally-driven flow.

Yankovsky and Chapman (1997) classified plumes as "surface-advected," in which the plume is relatively shallow and the flow is dictated by surface dynamics, or "bottom-advected" in which the plume extends to the bottom and its offshore extent and velocity structure is dictated by bottom Ekman dynamics and thermal wind balance. Using only discharge parameters, Yankovsky and Chapman (1997) were able to predict the fate of waters within the plumes. They showed that the behavior of the plume can be predicted based on the relationship between the predicted depth of the plume, h_b, expressed as:

$$h_b = \sqrt{\frac{2fQ_R}{g'}} \tag{8}$$

and the mean depth of the region. A value of h_b that is less than the mean depth of the region indicates a "surface-advected" plume and a value of h_b that is greater than the mean depth of the region indicates a "bottom-advected" plume.

The shallow nature of "surface-advected" plumes can make them susceptible to mixing and advection from winds (e.g. Fong and Geyer 2001; Whitney and Garvine 2005; Pinones et al. 2005). A measure of the competing mechanisms of advection and mixing can be achieved by dividing the Rossby number by the Ekman number, producing a plume Reynolds number:

$$Re_p = \frac{R}{E_k} = \frac{u_c h_p^2}{K_z R_D} \tag{9}$$

Large values of the plume Reynolds number ($Re_p>1$) indicate advection processes are dominant, while small values ($Re_p<1$) indicate frictional or mixing processes dominate. The susceptibility of the plume to overturning can be estimated using a measure of the relative strengths of stratification and vertical mixing: the Richardson number (e.g. Kato and Phillips 1969; Kantha et al. 1977), R_i, which is expressed as:

$$R_i = \frac{g'\Delta z}{(\Delta u)^2} \tag{10}$$

where Δu is the absolute difference between velocities at two different depths and Δz is the distance between the two depths. Values of R_i less than 0.25 typically indicate that the kinetic energy of the flow can overcome the vertical stratification and mix the plume (Smyth and Moum 2000; Sanders and Garvine 2001).

Materials and Methods

Study Site

Our investigation was conducted over a three year time period from August 2006 to June 2009 in the mouth of the Saco River and the adjacent Saco Bay (Fig. 1). The Saco River is located in the southwestern Gulf of Maine and is the 6th largest river discharging into the coastal waters of the Gulf of Maine, with a discharge rate that can exceed 600 m^3s^{-1} during spring runoff events. It enters the Gulf of Maine through a relatively narrow mouth (approximately 250 m) flanked by two jetties, resulting in a discrete point of entry. The Saco River Estuary is a partially mixed estuary. Its discharge extends into the relatively open Saco Bay (Kelley et al. 2005) and is the primary source of freshwater for that bay. The Saco River typically generates a plume that is 1–2 m deep and highly mobile. Tidal range is 2.7 m. The offshore edge of the region is affected by the southwestward flowing Western Maine Coastal Current (WMCC), a component of the river-driven coastal current system located along the western edge of the Gulf of Maine (Pettigrew et al. 1998; Geyer et al. 2004).

Hydrographic Surveys

We performed approximately weekly surveys of the Saco River plume and the adjacent coastal region using a

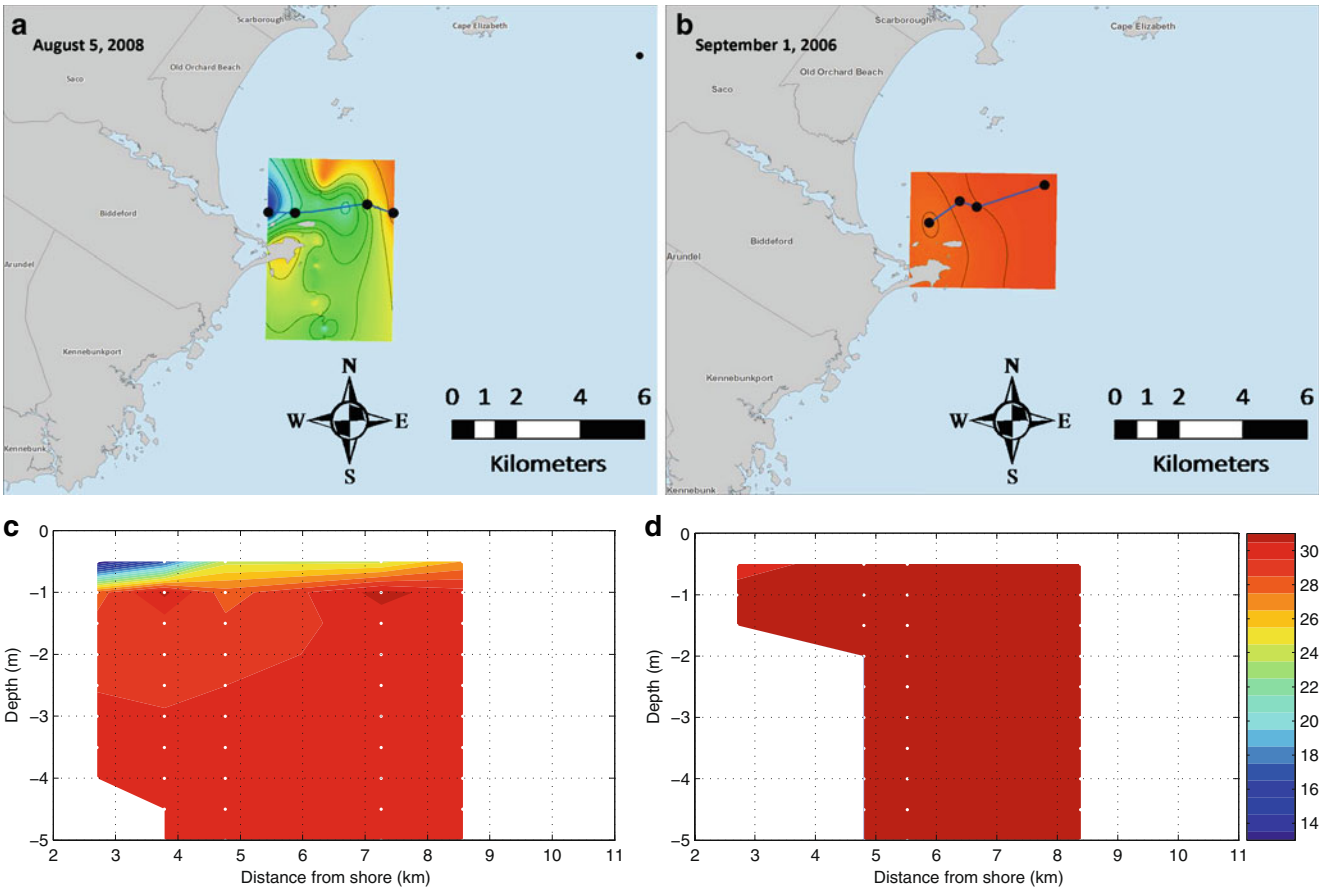

Fig. 1 Areal extent of the buoyant plume during **a** high discharge and **b** low discharge. Colored contours represent salinity. Black filled circles indicate the locations of CTD casts and thermosalinograph measurements used in the generation of the color contours. The blue lines in the upper panel indicate the paths of the cross-sectional views shown in the lower panel. Cross-sectional view of the plume during **c** high discharge and **d** low discharge

manually deployed Seabird SBE 25 Sealogger CTD (Conductivity-Temperature-Depth instrument) and SBE 19plus V2 SEACAT CTD to document the vertical structure (and determine mean depth) of the plume and a SBE 45 MicroTSG thermosalinograph to document the horizontal surface structure (and determine the eastward edge) of the plume. Sampling followed an adaptive strategy designed to capture the offshore edge of the plume. A total of 49 surveys were performed between April and October over the 3-year period. The majority of the surveys consisted of east–west transects that encompassed the plume and a segment offshore of the plume; however, a number of more extensive surveys that encompassed both the northward and eastward extent of the plume were also completed. The location and structure of the plume can be affected by tides (e.g. Garvine 1974) and the strong diurnal winds (Pinones et al. 2005). Consequently, surveys were conducted in the morning and afternoon to capture effects of both the land- and sea-breeze and throughout the tidal cycle to capture effects of flood, ebb, and slack tides. Because salinity of the plume and the ambient coastal ocean varied seasonally, the eastward edge of the plume could not be identified by a fixed salinity value but was instead determined by the steepest horizontal gradient in surface salinity along the east–west transects. The size of the plume was a strong function of discharge, so we expressed locations within the plume as functions of Rossby radius and not set distances. Here, "far-field" refers to parts of the plume that are located at least $1R_d$ away from the mouth, while "near-field" refers to portions of the plume that are located within $1R_d$ from the mouth.

Moored Instruments

Time series data used in this study were acquired from the Saco River Coastal Observing System (SaRCOS), which consists of a shore-mounted mooring located at the mouth of the river (not used in this study) and an ocean mooring (hereafter referred to as the SaRCOS mooring) that was located approximately 1 km east of Wood Island (Fig. 1). The ocean mooring consisted of an Aanderaa RCM-9LW current meter that measured velocity, salinity, and temper-

ature (at 1 m depth), a SBE 16PIM Seacat CTD that measured salinity, temperature, pressure, and fluorescence (colored dissolved organic matter, turbidity, chlorophyll; at 3 m depth), two SBE 37-IM MicroCat CTDs that measured salinity, temperature, and pressure (at 8 and 12 m depths), and two SBE 37-IM MicroCat CTs that measured salinity and temperature (at 5 and 22 m depths). In the spring of 2009, a downward looking 600 kHz RDI Workhorse Acoustic Doppler Current Profiler (ADCP) was installed (at 2 m depth) on the mooring to improve the vertical resolution of the velocities. All mooring data were collected at 20 min intervals. The conductivity sensor on the Aanderaa RCM-9LW experienced significant biological fouling due to the settlement of barnacles and hydroids each spring and summer. Consequently, the time series for surface salinity was limited to times before or after the fouling period or when fouling organisms had been manually removed. Since the irregular coastline (and associated islands) did not allow for a straight-forward determination of along- and across-shelf directions, velocities were converted to eastward and northward components.

Other Data

Wind measurements in this study were obtained from the National Oceanic and Atmospheric Administration (NOAA) environmental buoy EB 44007, located 15 km northeast of the study site. Wind data were collected at 20 min intervals. Surface salinity measurements were also obtained from GoMOOS mooring "C," located 24 km upshelf of the region within the WMCC (Pettigrew et al. 2005). Wind stress was calculated using the formulation by Large and Pond (1981). Daily river discharge data were obtained from the US Geological Survey gauging station at Cornish, ME. The discharge data were corrected for drainage areas downstream of the gauging station by dividing the total drainage area of the watershed by the discharge area upstream of the gauging station (e.g. Anderson et al. 2005).

Data Analysis

Salinities, velocities, and winds were examined using spectral and coherence analysis. The confidence levels and intervals for correlations, coherence, and spectra were computed following the methods described by Emery and Thomson (2001). Every reported correlation coefficient is significantly different from zero at the 95% confidence level. For the moored and wind data series, the degrees of freedom (N_{eff}) replaced the number of observations (N) in determining significance. N_{eff} was calculated by dividing the total time of the observations by the time of the first zero crossing of the autocorrelation function (e.g. Bretherton et al. 1999). Principal component and harmonic tidal analysis were performed on surface velocity data to determine the direction of maximum variance and the tidal velocities. To remove high-frequency diel and tidal variations prior to correlation calculations, the winds, currents, and salinity data sets were filtered using a Lanczos low-pass filter with a cut-off frequency of 1/36 h^{-1} (Jones and Epifanio 1995). Since the region was affected by large variation in discharge, calculations were performed for river flows grouped into high discharge (>500 m^3/s), low discharge (<65 m^3/s) and moderate discharge (all other values) periods.

Results

Representative areal plots and vertical cross-sections of the region show a plume that varies due to discharge (Fig. 1) and wind direction (Fig. 2). Salinities in the plume during low discharge varied from a low of 26 at the surface of the plume to a high of 33 in the ambient waters (right panel of Fig. 1). Under high discharge conditions, there was much greater range (both horizontal and vertical) in salinity, varying between 13 and 33 (left panel of Fig. 1); however, the plume thickness remained between 1 m and 2 m for all conditions. The effect of winds on the plume was not consistent with Ekman dynamics. Surveys of the plume during periods of comparable discharge and wind speeds, but different wind directions (see illustrative examples in Fig. 2), reveal large differences between the offshore extent of the plume. Northward winds (which would tend to move the plume northward and offshore in Ekman dynamics) *reduced* the offshore extent of the plume (Fig. 2b). Southward winds (which would tend to move the plume southward and onshore in Ekman dynamics) *increased* the offshore extent of the plume (Fig. 2a).

Examination of the discharge measured at the USGS gauging station at Cornish, ME (Fig. 3a) reveals strong temporal variability in river outflow. Discharge varied between 40 m^3/s and 620 m^3/s during the study period. Discharge was greatest during the spring freshet that occurs during April and May of each year. Additional, smaller peaks also occurred in the falls of 2006 and 2008 due to increased storm activity (mainly the remnants of tropical storms) during these periods. There was also considerable interannual variability. Conditions were wetter and river discharge greater in 2006 and 2008 than in 2007.

Although the biological fouling of the Aanderaa conductivity sensor prevented continuous coverage of the surface salinity, the time series of salinity data at the different depths did encompass portions of spring, summer, and winter, and exhibited strong interannual, seasonal, and daily variability. Salinity trends at three representative

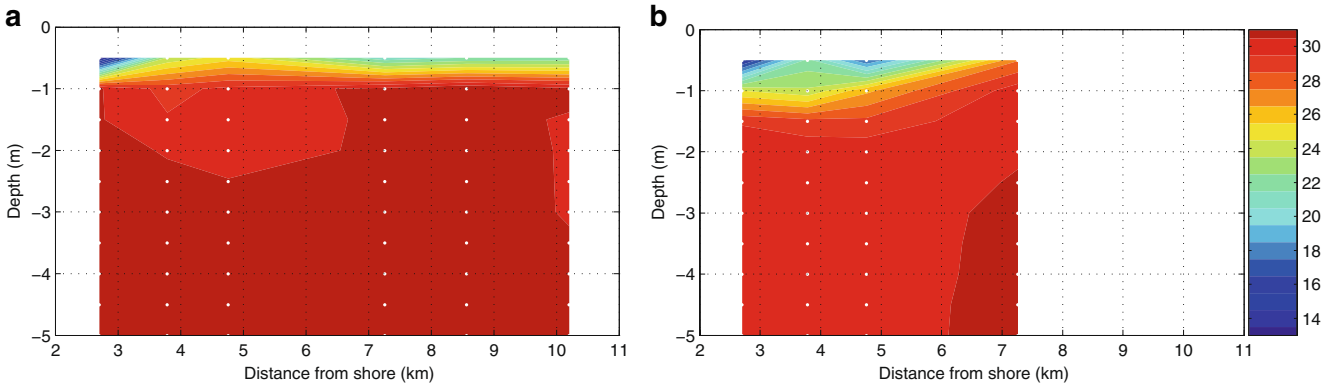

Fig. 2 Cross-sectional view of the plume during **a** southward winds and **b** northward winds

depths (1, 5, and 22 m depth) are shown in Fig. 3b. Although additional salinity measurements (at 3, 8, and 12 m) are available, they closely track the representative depths shown, with salinity at 3 m and 8 m reflecting salinity at 5 m and salinity at 12 m closely following salinity at 22 m. This pattern indicates a shallow, surface plume and little vertical stratification below the plume. Salinity values were at their lowest during the spring freshet of each year and surface salinity periodically dropped below 20. Salinity was significantly higher during the summers and winters when discharge was at its lowest (Fig. 3b). The time series of salinity values at the mooring was consistent with the vertical cross sections, indicating fresher water at the surface and more saline water at depth. Comparison of mean salinity during high (discharge >500 m^3/s), low (discharge <65 m^3/s), and moderate (all others) river discharge reveals an inverse relationship between discharge and salinity in the region

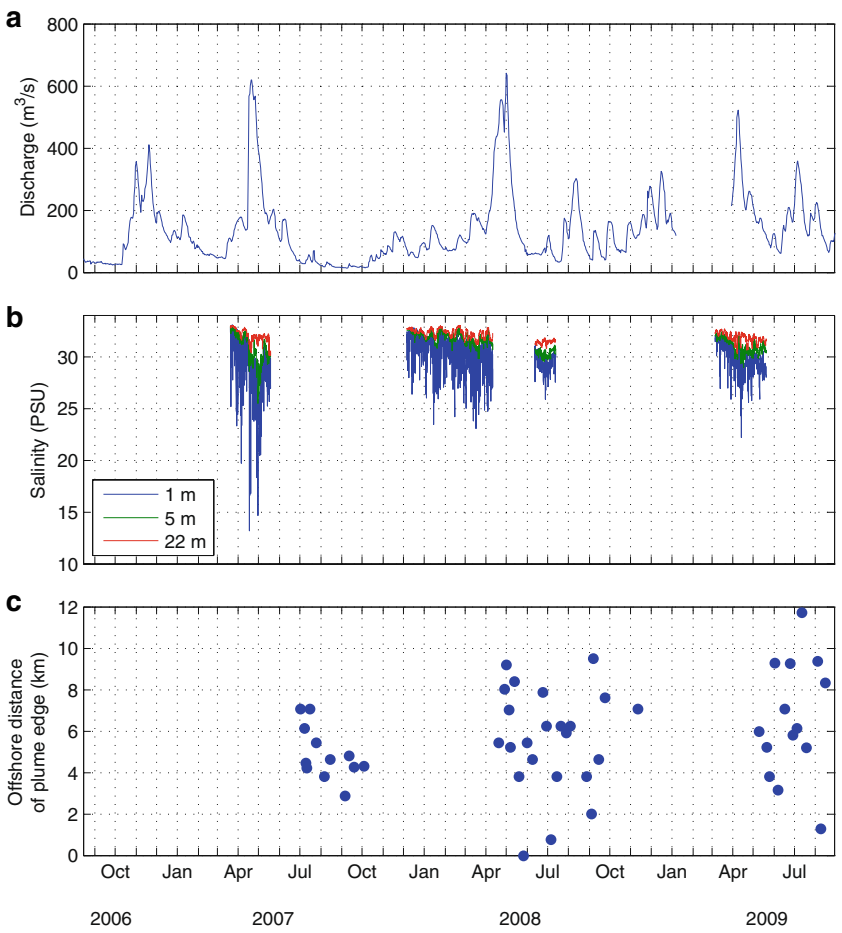

Fig. 3 Time series of **a** discharge (m^3/s) obtained from the Cornish, ME USGS gauging station, **b** the salinity at depths of 1, 5, and 22 m at the SaRCOS mooring, and **c** offshore location of the eastern plume boundary (km) as a function of time. The lack of discharge data during late spring 2009 was due to the presence of ice at the gauging station

(Table 1). Low discharge resulted in high salinity and little vertical stratification, while high discharge resulted in low salinity and large vertical stratification. Correlations between salinity and discharge were negative (high discharge leads to low salinity) as expected; however, the low values of correlation indicate that other mechanisms affect salinity fluctuations in the region.

The location of the offshore edge of the plume varied between the mouth of the river during lowest discharge to over 10 km offshore during some wind conditions or extremely high discharge (Fig. 3c). The correlation (with a 1 day lag) between offshore extent of the plume and discharge was 0.42. To determine the relationship between winds and plume movement, we compared the offshore extent or edge of the plume with the projection of the observed wind velocity vector in each direction. The highest correlation between wind velocities and offshore extent (0.45, lag=22 h) occurred when winds were oriented towards 215°T, which is approximately downshelf.

Examination of the surface velocities revealed a southeastward mean flow that varied from 0.08 m s^{-1} during low discharge to 0.17 m s^{-1} during high discharge (Fig. 4a). Principal component analysis of velocity revealed that the greatest variation coincided with the direction of mean flow and correlated with discharge (Fig. 4b). The proximity of the mooring to the mouth of the river resulted in mean flow that was not oriented parallel to the coastline but instead directed away from the mouth. Harmonic tidal analysis revealed M2 tidal velocities that were comparable or less than the mean flow. The major tidal axis (Fig. 4c) did not coincide with the direction of greatest variation in velocity, indicating other factors such as discharge and wind-driven processes affected flow in the region.

Power spectra of salinity time series (Fig. 5a) reveal strong variation at low frequencies at all depths and at M2 (1/12.42 h^{-1}) and M4 (1/6.21 h^{-1}) tidal frequencies (corresponding to 1.9 and 3.9 cpd, respectively) at 1 m and 22 m depths. Interestingly, there was no variation in salinity at the 5 m depth at the expected tidal frequencies. The velocity power spectrum (Fig. 5b) shows strong fluctuations at the tidal frequencies as well as some significant variation at 0.2–0.3 cpd (3–5 days) that are consistent with wind fluctuations for the 1 m velocities; however, the velocity spectra at 5 and 22 m show fluctuations only at tidal frequencies. The wind velocity power spectrum (Fig. 5c) shows significant variation only at a diurnal time period (1 cpd) most likely associated with the sea breeze.

We examined the eastward and northward winds separately to determine any change in the ocean's response to the different forcings (Geyer et al. 2004). The winds and currents were filtered to remove diel and tidal frequency variations before correlation coefficients were calculated. Correlations for both components were higher for wind velocities than wind stress, which is consistent with previous studies (e.g., Garvine 1991; Whitney and Garvine 2005; Warrick et al. 2007). Eastward wind velocity was most highly correlated with surface eastward currents (r= 0.62, lag=0 h), consistent with downwind frictional movement in a nearshore environment (Tilburg 2003). Northward wind velocity was most highly correlated with surface currents oriented toward 35°N (r=0.71, lag=0 h), suggesting a combination of Ekman dynamics and induced geostrophic motion (Geyer et al. 2004). Linear regression indicated that the correlated currents were 1.3% and 2.1% of the eastward and northward wind velocity, respectively. These relationships are compatible with the "mariner's rule" that wind-driven currents are a few percent of wind speed (Tilburg and Garvine 2003). Currents at 4 m and below were not significantly correlated with winds, indicating that the depth of penetration of wind stress (<4 m) was comparable to the plume thickness (1–2 m).

Coherence between salinity variation at 1 m and the surface currents was significant at the M2 and M4 tidal periods as well as 3–5 day time scales (0.2–0.3 cpd) of wind forcing, and longer time scales (<0.05 cpd) most likely associated with seasonal variation in discharge (Fig. 6a). Phase spectra were also calculated for coherence between salinity and surface currents (not shown). Phases of significant coherence between salinity and velocity occurred between −140° and −160° for eastward velocities (maximum coherence between eastward flow and reduced salinities would result in a phase of −180°) and between 50° and 70° for northward velocities (maximum coherence between northward velocities and reduced salinities would result in a phase of 180°), indicating that eastward and southward (to a lesser extent) velocities (i.e. those that would transport fresh river water to the mooring) resulted in decreased salinity. Interestingly, there was no coherence

Table 1 Salinity values at SaRCOS mooring

Depth	Low discharge	Moderate discharge	High discharge	Correlation between salinity and discharge	Time lag (days)
1 m	30.95	29.96	27.75	−0.33	0
5 m	31.54	31.31	30.38	−0.22	0
22 m	32.04	32.04	31.74	−0.13	0

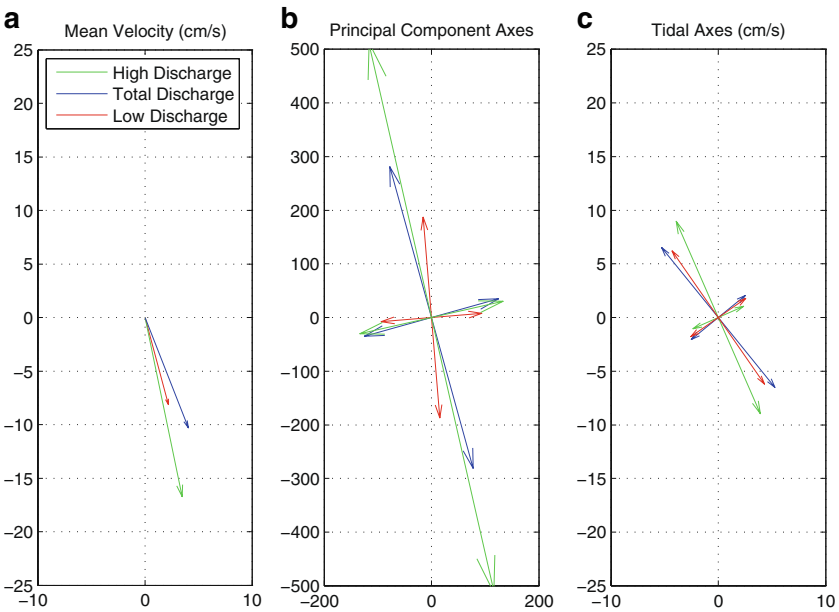

Fig. 4 Mean velocity (cm/s) (**a**), principal component axes (**b**), and tidal axes (cm/s) (**c**) of the surface velocities at the SaRCOS mooring

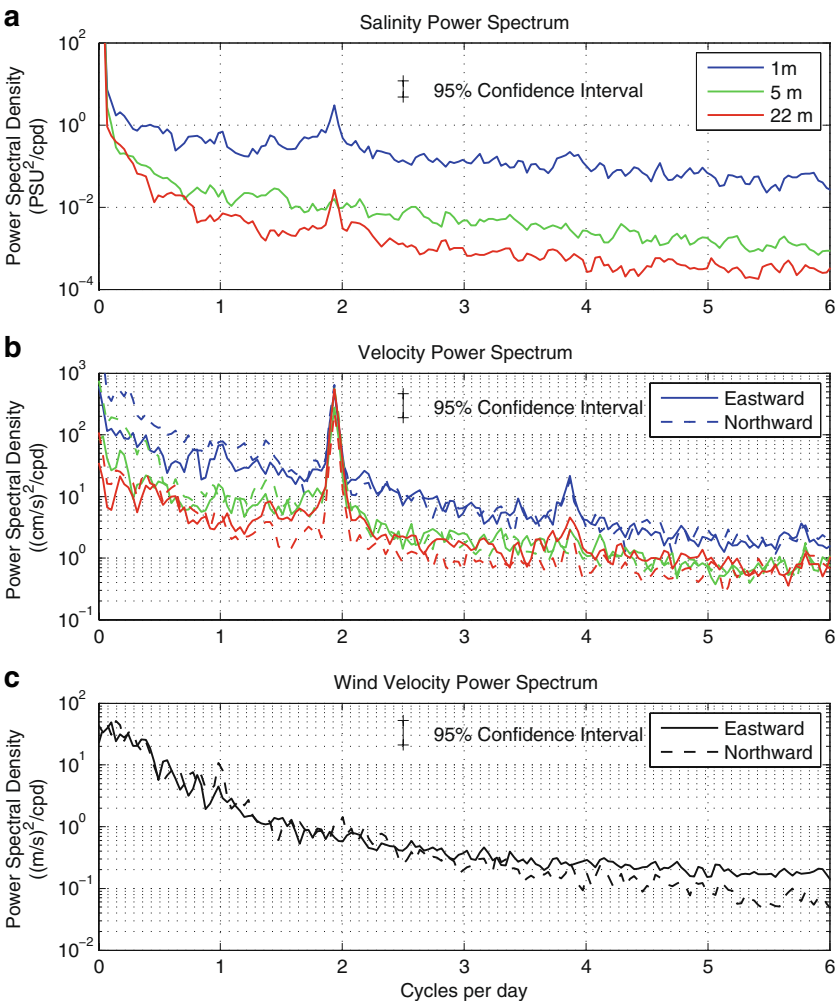

Fig. 5 Power spectra of salinities (**a**) and velocities (**b**) at depths of 1, 5, and 22 m, and surface wind velocities (**c**). Spectra were created using a Welch spectral estimation method. Spectral calculations were made with 95% confidence intervals

between salinity and surface velocities at 1 cpd that would be consistent with the effects of the sea breeze (e.g. Pinones et al. 2005). Although there is energy within the wind field at 1 cpd (Fig. 5c), the absence of coherence suggests that the complex geometry of the coastline (Fig. 1a) tends to complicate the small-scale on- and offshore downwind movement of the plume, preventing wind-forced diurnal variation of the salinity within the plume.

The effect of winds on salinity did not extend to greater depths. There was no coherence between salinity and velocity at the 3–5 day time scales for depths ≥5 m. (Fig. 6b and c). Coherence was significant at tidal and seasonal frequencies for 22 m (Fig. 6c) but only seasonal frequencies for 5 m (Fig. 6b). Coherence was also significant at approximately 1.4–1.5 cpd for 5 m, although it is not clear what forcing drives the high coherence at these higher frequencies. The coherence between surface salinity and winds was consistent with wind-driven flow; the highest (although not significant) coherence occurred at 3–5 day time scales.

Correlations between the salinity at the SaRCOS mooring and surface salinity at the GoMOOS mooring "C" (which is located within the WMCC, 24 km upshelf of the SaRCOS mooring) were significant (for at least some time lags) at all depths (Fig. 7, Table 2). However the strongest correlation between mooring "C" and the SaR COS mooring occurred at the 5 m depth and was higher than the correlation between any two depths within the SaRCOS mooring (Table 2). Maximum correlations of salinity at depths of 1 and 5 m exhibited a time lag of 1.2 days, while correlation of salinity at a depth of 22 m was highest from 0 to 0.7 days (Fig. 7). The distance between mooring "C" and the SaRCOS mooring (≈24 km) should result in sizable time lags in the salinity signal. Geyer et al. (2004) found that downshelf velocities within the WMCC varied between 0.2 m/s and 0.4 m/s. Using

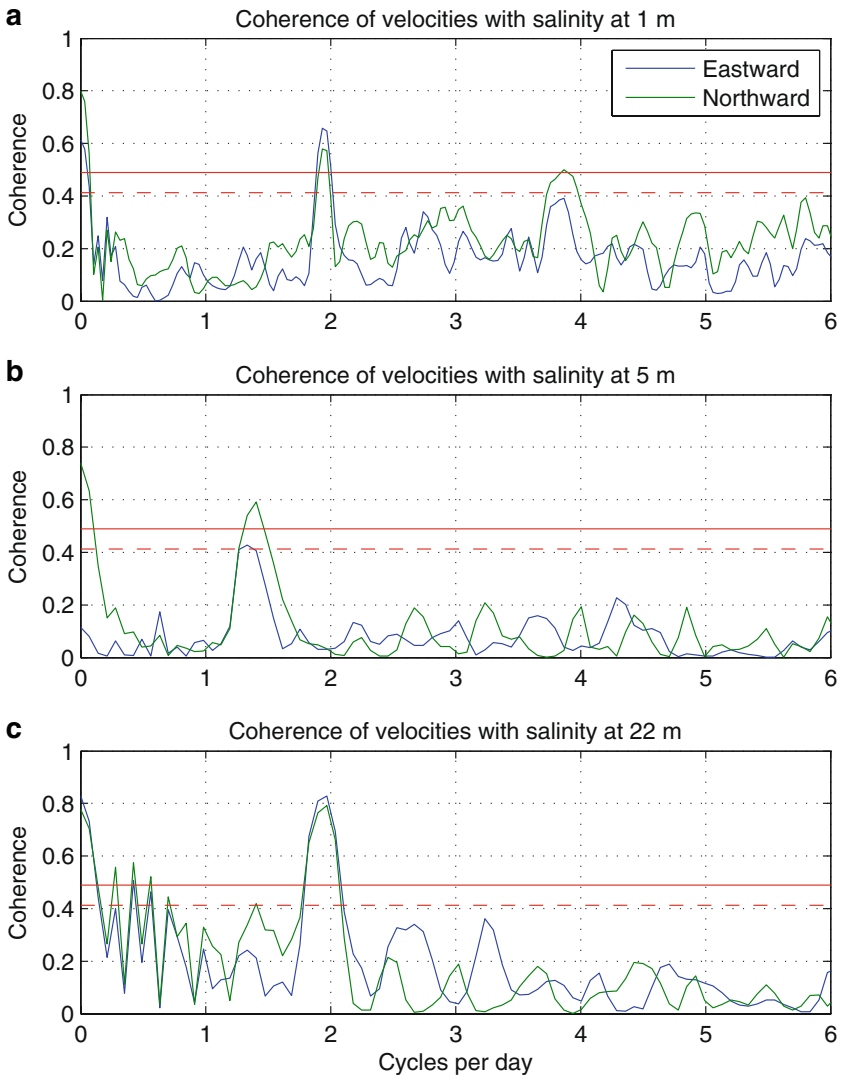

Fig. 6 Coherence of velocities with salinities at depths of 1 m (**a**), 5 m (**b**), and 22 m (**c**). *Red lines* indicate 95% (*solid line*) and 90% (*dashed line*) significance. Levels of significance were calculated using an estimated N_{eff}=16

these speeds as estimates of the propagation speed of the salinity signal in the WMCC, the expected lag time of the maximum salinity correlation was between 0.7 and 1.4 days, which encompasses the observed time lags (Fig. 7).

Values of several parameters that describe the general characteristics of the plume (Garvine 1995; Yankovsky and Chapman 1997) for high, moderate and low discharge (Table 3) suggest that changes in river discharge can result in dramatically different dynamics that govern the propagation and structure of the plume. The ranges in river discharge result in large variation in the tidal index, P, indicating that the flow is buoyancy dominated ($P>1$) during high discharge and tidally driven ($P<1$) during low discharge (Table 3). Examination of K indicates that ranges in river discharge result in dramatically different dynamics in the far-field. During high discharge, the plume extends further offshore (R_p~9 km) and affects a larger portion of the bay. The greater spatial extent of the plume allows for rotational processes to dominate ($K>1$) within the plume away from the mouth. During low and moderate discharge, the plume is smaller ($R_p<2$ km), resulting in inertial processes dominating throughout the plume (Table 3). Values of Rossby number are consistent with observed values of K. For low discharge, R~1, indicating both inertial and rotational processes were important, but at high discharge, $R<1$, indicating rotational processes dominated within the plume. Using a typical value of vertical eddy viscosity (~2.0×10^{-4} m^2/s) found within coastal river plumes (e.g. Houghton et al. 2004; Fong and Geyer 2001), the Ekman number was calculated to be 0.5, indicating that rotational processes predominate over frictional processes. Examination of Fr reveals that stratification was important at all times within the plume. Dynamics near the mouth differed from those within the body of the plume. The small inlet of the Saco River (W= 250 m) resulted in small values of K_m for all discharges (Table 3, 0.075–0.17), indicating that the region near the mouth is affected by inertial processes and the discharge is likely to form a bulge (Geyer et al. 2004; Garvine 1999) with low salinities both up- and downstream of the mouth. However, values of R_m were small, indicating that rotational processes were also important near the mouth. Examination of Fr_m reveals that during high discharge, inertial processes were more important than stratification near the mouth, but at lower discharges, stratification was more important in governing the flow.

Calculated values of h_b (Yankovsky and Chapman 1997) are consistent with the observed thickness of the plume and indicate a "surface-advected" plume for all discharge values (Table 3). The shallow nature of the plume (~ 1–2 m depth) can make it susceptible to mixing and advection from winds. Plume Reynolds numbers were near 1 for all values of discharge indicating that both advection and mixing processes can be important. Richardson numbers were calculated using the density and velocity at 1 m and 4 m depths. Time series of the projection of wind velocity onto a vector oriented towards 215°T (Fig. 8a) and Richardson number (Fig. 8b) during an example period of moderate

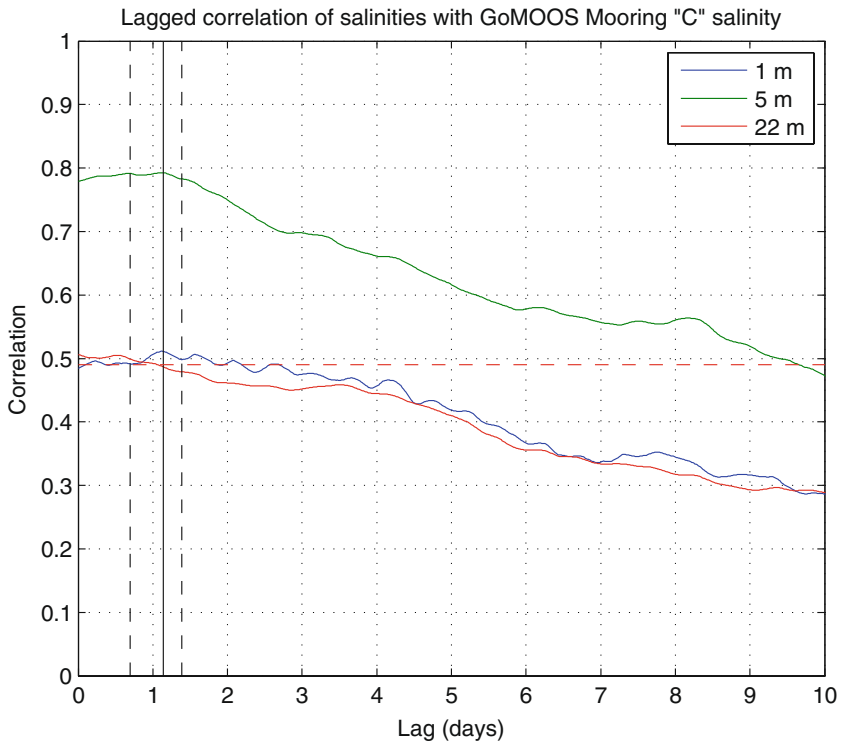

Fig. 7 Lagged correlation between salinity at different depths at the SaRCOS mooring and surface salinity at GoMOOS mooring "C." *Horizontal red dashed line* indicates 95% significance. *Black vertical line* indicates time lag of maximum correlation for 1 and 5 m salinities. *Black vertical dashed lines* represent minimum and maximum expected time lag calculated from propagation speeds in the WMCC

Table 2 Correlation values of salinities at SaRCOS and GoMOOS "C" moorings

	1 m	5 m	22 m	"C"
1 m	1	0.63	0.39	0.51
5 m		1	0.71	0.79
22 m			1	0.61
"C"				1

"C" mooring salinity was measured at a depth of 1 m

discharge (March 2009) show that during strong wind events *Ri* frequently falls below 0.25, indicating mixing of the plume with the ambient ocean. During high discharge (not shown), *Ri* rarely falls below 0.25, indicating that high discharge events do not typically mix the plume, despite the high *Fr* near the mouth.

Discussion

Characteristics of the Buoyant Flow

Observations and calculations indicated a shallow plume whose salinity and flow are strongly influenced by winds, tides, discharge, and the presence of the Western Maine Coastal Current. The size and character of the plume was a strong function of discharge. The dynamics of the plume changed from "small-scale," in which inertial effects dominated flow patterns throughout the plume during low discharge, to "large-scale," where rotational effects dominated in the far-field (i.e. $>1R_d$ away from mouth) during high discharge. Due to the small inlet, the effects of discharge on the dynamics of the flow were different near the mouth, where high discharge produced strongly inertial, supercritical flows, and low discharge resulted in subcritical flows. Low discharge resulted in a tidally-driven flow near the mouth, while high discharge resulted in a buoyancy-driven flow. Calculations of h_b revealed that the plume would be "surface-advected" for all discharge regimes (Table 3). The plume was rarely thicker than 1–2 m deep (indicating a "surface-advected" plume). Currents in the region were highly correlated with winds, revealing both a simple downwind (for eastward) and Ekman (for northward) response to the winds; however, the effects of winds were constrained to the surface due to the strong vertical stratification within the plume. The areal and vertical structure of the plume (Fig. 1) is consistent with the predicted characteristics of the plume. Low salinities were frequently detected up- and downshelf of the mouth (indicating near-field bulge formation); however, during high discharge, low salinities were found slightly upshelf but more than 4 km downshelf (indicating far-field geostrophic turning).

Interaction with the Western Maine Coastal Current

The significant coherence of surface velocity and salinity at the mooring at tidal frequencies indicates that the salinity is highly affected by tidal flow. Interestingly, the high coherence is confined to the shallowest (1 m) and deepest mooring (22 m) depths. Although the middle depth (5 m) exhibits strong variation in velocity at tidal frequencies (Fig. 5b), there is little variation in salinity (Fig. 5a) and no coherence at tidal frequencies (Fig. 6). The barotropic nature of tides should result in high correlations between salinity and tidal velocity at all depths in a region heavily

Table 3 Key parameters of the Saco River Plume

Parameter	Symbol	Low discharge	Moderate discharge	High discharge
Discharge (m^3/s)	Q_r	65	110	500
Tidal index	P	0.56	1.2	4.4
Reduced gravity (N/kg)	g'	0.015	0.036	0.075
Internal Rossby Radius (km)	R_D	1.5	2.3	3.4
Observed radius (km)	R_P	0.8	1.6	9.0
Mean speed (m/s)	u_{ave}	0.082	0.11	0.18
Bulk Kelvin number	K	0.53	0.69	2.7
Mouth Kelvin number	K_m	0.17	0.11	0.075
Rossby number	R	1.02	0.67	0.19
Mouth Rossby number	R_m	0.62	0.68	0.44
Ekman number	E_k	0.50	0.50	0.50
Froude number	Fr	0.54	0.46	0.52
Mouth Froude number	Fr_m	0.33	0.47	1.19
Plume Reynolds number	Re_p	1.09	0.95	1.06
Predicted depth (m)	h_b	0.81	0.78	1.0

$f=9.9\times10^{-5}$ s^{-1}, $W=250$ m

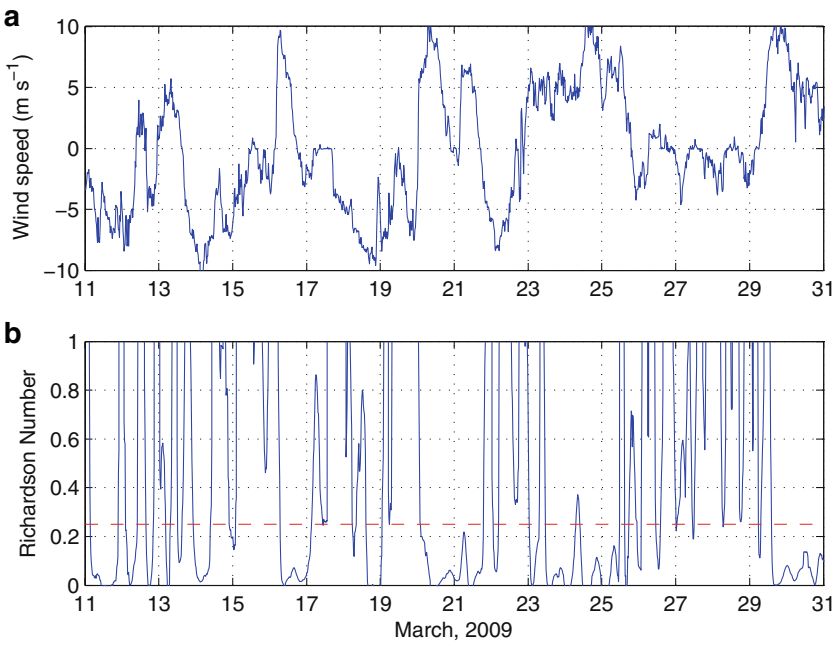

Fig. 8 **a** Projection of wind velocity onto a vector oriented toward 215°T. *Positive* indicates southwestward flow. *Negative* indicates northeastward flow. **b** Richardson number at SaRCOS mooring. *Red dashed line* indicates a Richardson number of 0.25

influenced by river discharge. However, examination of the large-scale flow field reveals that the offshore edge of the region is dominated by the southwestward flowing, baroclinic WMCC (Geyer et al. 2004; Churchill et al. 2005) whose flow is governed by geostrophic and wind-driven transport (Geyer et al. 2004; Hetland and Signell 2005). Recent studies of the WMCC show that it can penetrate shoreward of the SaRCOS mooring and generally extends to depths of 15–25 m (Geyer et al. 2004; Pettigrew et al. 2005). Salinity correlations between the SaRCOS mooring and the upshelf mooring "C" were stronger at 5 m (r=0.79) than at 22 m depth (r=0.61), suggesting that the SaRCOS mooring is strongly affected by the baroclinic WMCC, which does not always extend to the bottom in this region. The lack of coherence of salinity with tides at 5 m is consistent with the results of Geyer et al. (2004) who found weak tidal effects in the WMCC. Coherence of salinity with tides at 22 m (but not at 5 m) suggests that the WMCC that does not always extend to 22 m. The lack of coherence of salinity with winds at 5 and 22 m is consistent with the shallow Ekman depths created by the buoyant discharge from the Saco River. In contrast to our study, Geyer et al. (2004) found that the WMCC is strongly influenced by winds; however, their analysis did not extend to the highly stratified inshore regions such as those affected directly by the Saco River discharge.

Offshore Movement of the Plume

The offshore movement of the eastward edge of the buoyant plume is governed by the salinity field created by river discharge and vertical mixing due to winds. Higher discharge results in greater offshore movement, which is consistent with a small K_m and larger Fr_m, resulting in buoyant transport from the mouth that leads to bulge formation. Garvine (1999) showed that for small K_m, the discharge should create a bulge whose horizontal scale varies with river discharge. The positive, lagged correlation between discharge and offshore movement of the plume is consistent with the creation and subsequent expansion of a buoyant bulge of freshwater emanating from the mouth (Nof and Pichevin 2001).

The offshore movement of the plume due to winds is not a product of Ekman dynamics or even downwind advection of the plume. Plume Reynolds numbers of approximately unity for all discharges suggests that mixing due to winds is as important as advection. The highest correlation between offshore movement of the plume and winds (r=0.45, lag= 22 h) occurs when the wind component is oriented towards 215°T, which is not consistent with Ekman dynamics (in which maximum correlation would occur for northeastward winds) or downwind frictional advection (in which maximum correlation would occur for eastward winds). The relationship between winds and the offshore movement of the plume appears to be based on physical mechanisms that take time to develop; the time lag between winds and offshore plume extent (22 h) is greater than that expected for Ekman dynamics (Garvine 1991) in a region where the highest correlation between velocities and winds shows no time lag. There is not a significant correlation between the velocities at the mooring and the offshore extent of the plume, which suggests a physical mechanism other than

advection governing the edge of the plume. Since the plume edge results from a balance between the horizontal transport of buoyancy and the vertical mixing (Fong and Geyer 2001; Houghton et al. 2004), wind-driven vertical mixing can result in the eventual destruction of the plume edge, decreasing the offshore extent of the plume. Calculations of the Richardson number (Fig. 8) reveal that commonly encountered winds can mix the shallow plume with the ambient ocean. However, the plume extent is not governed simply by wind-mixing, since high discharge events that tend to produce large plumes are characterized by strong stratification that limits the ability of winds to mix the plume. The orientation of the coastline, the location of the associated islands, and the direction of the dominant flow field determine the direction of the winds that are most likely to mix the plume. A significant correlation between plume extent and the wind velocity component oriented towards 215°T shows that northeastward winds are most effective in vertically mixing the plume (reducing its across-shelf extent), while southwestward winds are the least effective in mixing the plume. Northeastward winds oppose the typical flow of the southwestward WMCC resulting in greater vertical shear and more mixing. Southwestward winds blow in the same direction as the WMCC, resulting in less vertical shear, less vertical mixing, and more advection of the plume.

The tombolo south of the Saco River mouth and Wood Island (which extend eastward to a longitude of 70.3°W or more than 6 km east of the main coast, labeled in Fig. 1) determine the extent to which the northeastward winds can mix the plume and modify the movement of the plume by southwestward winds. Examination of Fig. 2b reveals that northeastward winds mix the plume east of Wood Island, while the portion of the plume that resides in the lee of the island and tombolo is still intact. The presence of these features effectively shelters the plume from the mixing action of the northeastward winds. However, the tombolo and Wood Island play different roles for southwestward winds. Typically, downwelling winds tend to generate a strong downshelf flow while trapping a buoyant plume against the coast. Choi and Wilkin (2007), in a recent modeling study of the Hudson River plume, found that downwelling winds would decrease the across-shore extent of the plume by a factor of 2. Lentz and Largier (2006) in a study of the Chesapeake Bay plume showed that the across-shelf extent of the plume ranged from 2 to $3R_D$ during quiescent periods or upwelling events to less than $1R_D$ during downwelling events. For the Saco River plume, R_D varied between 1.5 km and 3.4 km. However, the presence of Wood Island interrupts this downshelf flow and forces the southwestward wind-driven flow to extend offshore of Wood Island before continuing downshelf. Since the seaward side of Wood Island is more than 6 km offshore (i.e. ~ 2–4R_D) of the river mouth, a plume that extends only $1R_D$ from shore is located much further eastward than a plume during quiescent or upwelling winds. The downshelf and subsequent offshore movement takes time to develop, consistent with the long lag time (22 h) between the onset of winds and offshore movement.

Summary and Conclusions

In this study, we examined the dynamics of the flow field of the Saco River plume in Saco Bay, Gulf of Maine using a combination of moored instruments and weekly transects of the region. Examination of observations of the plume revealed a shallow plume that is strongly influenced by winds, tides, discharge and the coastal current system along the western edge of the Gulf of Maine. The scale of the plume and therefore, the governing dynamics, were highly dependent on discharge. During high discharge, the spatial scales of the plume were larger than the radius of deformation, the effect of rotation was enhanced, and the far-field portions of the plume were affected by both inertial and rotational processes. During low discharge, the spatial scales of the plume were small, the effect of rotation was reduced, and the plume was dominated by inertial processes throughout the plume. Examination of characteristic parameters showed that the governing dynamics of the flow differed depending on the location within the plume. Near the mouth, high discharge resulted in inertial, supercritical flow, while low discharge resulted in weaker, subcritical flow.

The location of the plume was highly dependent on the strong tidal velocities in the region and the presence of the southwestward flowing WMCC that was present along the eastern edge of Saco Bay. The shallow plume was strongly affected by winds, although not by Ekman dynamics. The location of the plume was a product of both wind-induced vertical mixing and the presence of the island and tombolo located offshore of the river mouth. Strong northeastward winds, which would tend to transport the plume upshelf and offshore due to Ekman dynamics, instead mixed the plume with the ambient ocean, effectively reducing the across-shore extent of the plume. Southwestward winds would tend to result in downwelling and downshelf flow; however, the presence of Wood Island and a tombolo to the south redirected the downshelf flow to the east before it returned downshelf, effectively extending the eastward extent of the plume.

This study suffers from a number of limitations that can affect the interpretation of the measurements. Moored observations were confined to only one location within the plume and biological fouling did reduce the times at which surface data were available. Transects were confined

to spring, summer, and fall periods and did not necessarily coincide with mooring observations. Wave-driven transport was not addressed in this study but could be important to plume dynamics and dispersal of pathogens and toxins (Svejkovsky et al. 2010). However, our results present new insight into those physical mechanisms that can advect and mix plumes as well cause plumes to vary between "small-scale" and "large-scale" dynamics.

Acknowledgments The authors wish to thank the Maine Technology Institute for funding the equipment and the University of New England for funding the operating costs of the project. We would like to thank Michael Dunnington for help with the initial planning of the project and Kelly Provost, Christina Guidoboni, Theresa Robitaille, and Emily Zimmerman for assisting in the field. We are also grateful for the comments by two anonymous reviewers. This is contribution number 34 from the Marine Science Center at the University of New England.

References

Anderson, D.M., B.A. Keafer, W.R. Geyer, R.P. Signell, and T.C. Loder. 2005. Toxic *Alexandrium* blooms in the western Gulf of Maine: The plume advection hypothesis revisited. *Limnology and Oceanography* 50: 328–345.

Avicola, G., and P. Huq. 2001. Scaling analysis for the interaction between a buoyant coastal current and the continental shelf: Experiments and observations. *Journal of Physical Oceanography* 18: 1144–1166.

Bretherton, C.S., M. Widmann, V.P. Dyminikov, J.M. Wallace, and I. Blade. 1999. The effective number of spatial degrees of freedom of a time-varying field. *Journal of Climate* 12: 1990–2009.

Chao, S.-Y. 1988. Wind-driven motion of estuarine plumes. *Journal of Physical Oceanography* 18: 1144–1166.

Chao, S.-Y., and W.C. Boicourt. 1986. Onset of estuarine plumes. *Journal of Physical Oceanography* 16: 2137–2149.

Chapman, D.C., and S.J. Lentz. 1994. Trapping of a coastal density front by the bottom boundary layer. *Journal of Physical Oceanography* 24: 1464–1479.

Choi, B.-J., and J.L. Wilkin. 2007. The effect of wind on the dispersal of the Hudson River plume. *Journal of Physical Oceanography* 37: 1878–1897.

Churchill, J.H., N.R. Pettigrew, and R.P. Signell. 2005. Structure and variability of the Western Maine Coastal Current. *Deep-Sea Research Part II* 52: 2392–2410.

Cushman-Roisin, B. 1994. *Introduction to Geophysical Dynamics*. Englewood Cliffs, NJ: Prentice Hall.

Emery, W.J., and R.E. Thomson. 2001. *Data Analysis Methods in Physical Oceanography*, 2nd edition. Amsterdam: Elsevier Science.

Fong, D.A., and W.R. Geyer. 2001. Response of a river plume during an upwelling favorable wind event. *Journal of Geophysical Research* 106: 1067–1084.

Garvine, R.W. 1974. Physical features of the Connecticut River outflow during high discharge. *Journal of Geophysical Research* 79: 831–846.

Garvine, R.W. 1991. Sub-tidal frequency estuary-shelf interaction: Observations near Delaware Bay. *Journal of Geophysical Research* 96: 7049–7064.

Garvine, R.W. 1995. A dynamical system for classifying buoyant coastal discharges. *Continental Shelf Research* 15: 1585–1596.

Garvine, R.W. 1999. Penetration of buoyant coastal discharge onto the continental shelf: A numerical model experiment. *Journal of Physical Oceanography* 29: 1892–1909.

Gaston, T.F., T.A. Schlacher, and R.M. Connolly. 2006. Flood discharges of a small river into open coastal waters: Plume traits and material fate. *Estuarine, Coastal and Shelf Science* 69: 4–9.

Gersberg, R.M., D. Daft, and D. Yorkey. 2004. Temporal pattern of toxicity in runoff from the Tijuana River Watershed. *Water Research* 38: 559–568.

Geyer, W.R., R.P. Signell, D.A. Fong, J. Wang, D.M. Anderson, and B.A. Keafer. 2004. The freshwater transport and dynamics of the western Maine coastal current. *Continental Shelf Research* 24: 1339–1357.

Hansen, D.V., and M. Rattray Jr. 1966. New dimensions in estuary classification. *Limnology and Oceanography* 11: 319–326.

Henrichs, S., N. Bond, R. Garvine, G. Kineke, and S. Lohrenz. 2000. Coastal ocena processes CoOP: Transport and transformation processes over continental shelves with substantial freshwater inflows. Report on the CoOP Buoyancy-Driver Transport Processes Workshop.

Hetland, R., and R.P. Signell. 2005. Modeling coastal current transport in the Gulf of Maine. *Deep Sea Research Part II* 52: 2430–2449.

Houghton, R.W., C.E. Tilburg, R.W. Garvine, and A. Fong. 2004. Delaware River plume response to a strong upwelling favorable wind event. *Geophysical Research Letters* 31: L07302.

Huq, P. 2009. The role of Kelvin number on bulge formation from estuarine buoyant outflows. *Estuaries and Coasts* 32: 709–719.

Jones, M.B., and C.E. Epifanio. 1995. Metamorphosis of brachyuran megalopae in Delaware Bay: An analysis of time series data. *Marine Ecology Progress Series* 125: 67–76.

Kantha, L.H., O.M. Phillips, and R.S. Azad. 1977. On turbulent entrainment at a stable density interface. *Journal of Fluid Mechanics* 79: 753–768.

Kato, H., and O.M. Phillips. 1969. On the penetration of a turbulent layer into stratified fluid. *Journal of Fluid Mechanics* 37: 643–655.

Kelley, J.T., D.C. Barber, D.F. Belknap, D.M. Fitzgerald, S. van Heteren, and S.M. Dickson. 2005. Sand budgets at geological, historical and contemporary time scales for a developed beach system, Saco Bay, Maine, USA. *Marine Geology* 214: 117–142.

Large, W.G., and S. Pond. 1981. Open ocean momentum flux measurements in moderate to strong winds. *Journal of Physical Oceanography* 11: 324–336.

Lentz, S.J., and J. Largier. 2006. The influence of wind forcing on the Chesapeake Bay buoyant coastal current. *Journal of Physical Oceanography* 36: 1305–1316.

Lentz, S.J., and R. Limeburner. 1995. The Amazon River plume during AMASSEDS: Spatial characteristics and salinity variables. *Journal of Geophysical Research* 100: 2355–2375.

Lipp, E.K., R. Kurz, R. Vincent, C. Rodriguez-Palacios, S.R. Farrah, and J.B. Rose. 2001. The effects of seasonal variability and weather on microbial fecal pollution and enteric pathogens in a subtropical estuary. *Estuaries* 24: 266–276.

Munchow, A., and R.J. Chant. 2000. Kinematics of inner shelf motions during the summer stratified season off New Jersey. *Journal of Physical Oceanography* 30: 247–268.

Munchow, A., and R.W. Garvine. 1993. Buoyancy and wind forcing of a coastal current. *Journal of Marine Research* 51: 293–322.

Nagvenkar, G.S., and N. Ramalah. 2009. Abundance of sewage-pollution indicator and human pathogenic bacteria in a tropical estuarine complex. *Environmental Monitoring and Assessment* 155: 245–256.

Nof, D., and T. Pichevin. 2001. The ballooning outflows. *Journal of Physical Oceanography* 31: 3045–3058.

Otero, M.P., and D.A. Siegel. 2004. Spatial and temporal characteristics of sediment plumes and phytoplankton blooms in the Santa Barbara Channel. *Deep Sea Research Part II* 51: 1129–1149.

Pettigrew, N.R., D.W. Townsend, H. Xue, J.P. Wallings, P.J. Brickley, and R.D. Hetland. 1998. Observations of the Eastern Maine Coastal current and its offshore extensions. *Journal of Geophysical Research* 103: 30623–30639.

Pettigrew, N.R., J.H. Churchill, C.D. Janzen, L. Mangum, R.P. Signell, A. Thomas, D.W. Townsend, J.P. Wallinga, and H. Xue. 2005. The kinematic and hydrographic structure of the Gulf of Maine Coastal Current. *Deep Sea Research Part II* 52: 2369–2391.

Pinones, A., A. Valle-Levinson, D.A. Narvaez, C.A. Vargas, S.A. Navarrete, G. Yuras, and J.C. Castilla. 2005. Wind-induced diurnal variability in river plume motion. *Estuarine, Coastal and Shelf Science* 65: 513–525.

Rabalais, N.N., R.E. Turner, J. Dubravko, W. Dortch, W.J. Wiseman Jr., and B.K. Sen Gupta. 2000. Gulf of Mexico biological system responses to nutrient changes in the Mississippi River. In *Estuarine science: A synthetic approach to research and practice*, ed. J.E. Hobbie, 241–268. Washington, DC: Island.

Sanders, T.M., and R.W. Garvine. 2001. Fresh water delivery to the continental shelf and subsequent mixing: an observational study. *Journal of Geophysical Research* 106: 27087–27101.

Schiff, K.C., J. Morton, and S.B. Weisberg. 2003. Retrospective evaluation of shoreline water quality along Santa Monica Bay beaches. *Marine Environmental Research* 56: 245–253.

Simpson, J.H., and A.J. Souza. 1995. Semi-diurnal switching of stratification in the Rhine ROFI. *Journal of Geophysical Research* 100: 7037–7044.

Smyth, W.D., and J.N. Moum. 2000. Anisotropy of turbulence in stably stratified mixing layers. *Physical Fluids* 12: 1343–1362.

Svejkovsky, J., N.P. Nezlin, N.M. Mustain, and J.B. Kuma. 2010. Tracking stormwater discharge plumes and water quality of the Tijuana River with multispectral aerial imagery. *Estuarine, Coastal and Shelf Science* (in press).

Thomas, A.C., and R.A. Weatherbee. 2006. Satellite-measured temporal variability of the Columbia River plume. *Remote Sensing and the Environment* 100: 167–178.

Tilburg, C.E. 2003. Across-shelf transport on a continental shelf: do across-shelf winds matter? *Journal of Physical Oceanography* 33: 2675–2688.

Tilburg, C.E., and R.W. Garvine. 2003. Three-dimensional flow in a shallow coastal upwelling zone: Alongshore convergence and divergence on the New Jersey shelf. *Journal of Physical Oceanography* 33: 2113–2125.

Venkatesan, M.I., N. Chalaux, J.M. Bayona, and E. Zeng. 1998. Butyltins in sediments from Santa Monica and San Pedro basins, California. *Environmental Pollution* 99: 263–269.

Wargo, A.M., C.E. Tilburg, W.B. Driggers, and J.A. Sulikowski. 2009. Effect of a freshwater plume on icthyoplankton distribution off the coast of southern Maine. *Northeastern Naturalist* 16: 647–654.

Warrick, J.A., L. Washburn, M.A. Brzezinski, and D.A. Siegel. 2005. Nutrient contributions to the Santa Barbara Channel, California, from the ephemeral Santa Clara River. *Estuarine, Coastal and Shelf Science* 62: 559–574.

Warrick, J.A., P.M. DiGiacomo, S.B. Weisberg, N.P. Nezlin, M. Mengel, B.H. Jones, J.C. Ohlmann, L. Washburn, E.J. Terrill, and K.L. Farnsworth. 2007. River plume patterns and dynamics within the Southern California Bight. *Continental Shelf Research* 27: 2427–2448.

Whitney, M.M., and R.W. Garvine. 2005. Wind influence on a coastal buoyant outflow. *Journal of Geophysical Research Oceans* 110: C03014.

Yanagi, T., and T. Hino. 2005. Short term, seasonal, and tidal variations in the Yellow River plume. *Mer* 43: 1–7.

Yankovsky, A.E., and D.C. Chapman. 1997. A simple theory for the fate of buoyant coastal discharges. *Journal of Physical Oceanography* 27: 1386–1401.